iScience

CellPress
OPEN ACCESS

Article

In-depth understanding of boosting salinity gradient power generation by ionic diode

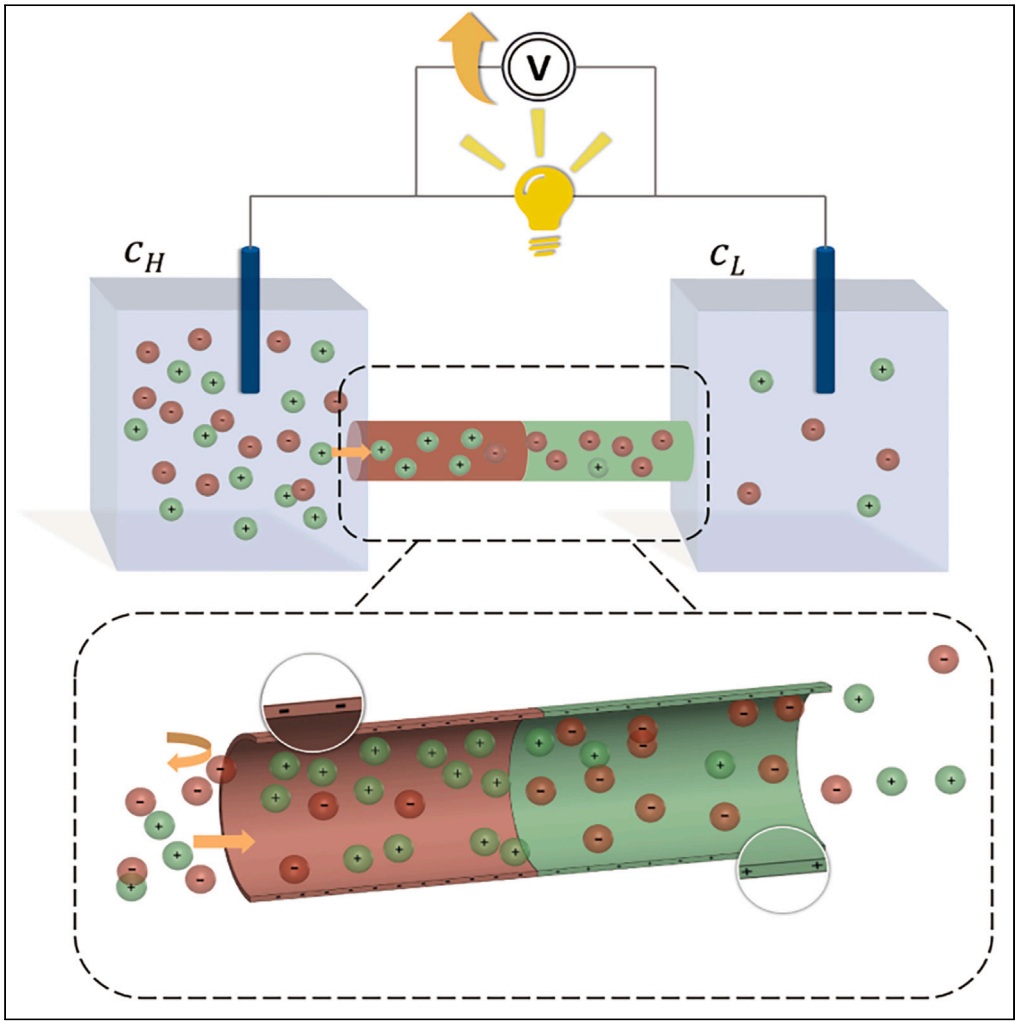

Ran Peng, Tong Li, Hanqiong Song, Shiyao Wang, Yongxin Song, Junsheng Wang, Minyi Xu

rpeng@dlmu.edu.cn (R.P.)
xuminyi@dlmu.edu.cn (M.X.)

Highlights

A model of bipolar ionic diode nanochannel for RED energy harvesting is presented

Bipolar ionic diode system gives higher maximum output voltage and output power

Prominent ion transport control of ion diode leads to outstanding RED performance

Optimization of RED harvester can be achieved by optimization of the ionic diode

Peng et al., iScience 26, 107184
July 21, 2023
https://doi.org/10.1016/j.isci.2023.107184

iScience

CellPress
OPEN ACCESS

Article

In-depth understanding of boosting salinity gradient power generation by ionic diode

Ran Peng,[1,5,*] Tong Li,[1,2,5] Hanqiong Song,[1] Shiyao Wang,[3,4] Yongxin Song,[1] Junsheng Wang,[3,4] and Minyi Xu[1,2,6,*]

SUMMARY

Ionic diodes constructed with asymmetric channel geometry and/or charge layout have shown outstanding performance in ion transport manipulation and reverse electrodialysis (RED) energy collection, but the working mechanism is still indistinct. Herein, we systematically investigated RED energy conversion of straight nanochannel-based bipolar ionic diode by coupling the Poisson-Nernst-Planck and Navier-Strokes equations. The effects of nanochannel structure, charging polarity, and symmetricity as well as properties of working fluids on the output voltage and output power were investigated. The results show that as high-concentration feeding solution is applied, the bipolar ionic diode-based RED system gives higher output voltage and output power compared to the unipolar channel RED system. Under optimal conditions, the voltage output of the bipolar channel is increased by ~100% and the power output is increased by ~260%. This work opens a new route for the design and optimization of high-performance salinity energy harvester as well as for water desalination.

INTRODUCTION

The use of renewable and clean energy shows great significance for the survival and sustainable development of human civilization. Salinity energy utilizing the concentration gradient of salt solutions has been considered as a promising renewable energy because of the abundant salty water resources over the world.[1–3] Two most commonly used methods, reverse electrodialysis (RED)[4–6] and pressure retarded osmosis (PRO),[7–9] have been applied in salinity gradient energy harvesting; but RED can convert salinity energy into electricity directly without additional pressure input and mechanical setup which is more popular than PRO.[10,11] In a RED system, a concentration gradient is built along an ion-select nanofluidic channel, and ions are driven by chemical potential and transport through the nanochannel; however, the transport of counter-ions through the ion-selective channel is promoted and transport of co-ions through the ion-selective channel is inhibited because of electrostatic attraction and repulsion caused by the presence of charges on the channel surface, thus resulting in a net charge stream in the nanochannel and giving an electrical energy output.[5,12,13] The concept of RED was first presented by Pattle in 1954 and has received reawakened attention in the field of nanofluidics because of the increasing development of nanotechnology.[14] To date, the energy conversion efficiency of RED is still very limited, and there is still a gap to reach the commercially viable performance benchmark of 5 W/m^2[10], especially to the large-scale applications of RED systems. Fundamental understanding and promotion of ion transport through nanochannels of RED systems is urgently needed to enhance the conversion efficiency which would guide the design and optimization of new RED systems.

To boost the performance of RED, numerous studies have been conducted, mainly focused on the properties of working electrolytes,[15,16] surface charge properties of the nanochannels,[15,17] and structure of nanochannels,[18–20] and so on. For instance, it is widely accepted that a higher surface charge density of the nanochannel would give rise to better ion selectivity thus a better RED energy conversion capability.[5] Also, well-matched electrolyte valence,[21] concentration,[22,23] and pH environment[24,25] are critical to high-efficiency power and energy conversion. Besides, the layout of the ion-selective nanochannel including shape, size, and symmetricity of charge modification also affects the performance of the RED system.[5,21,26] For example, Tseng et al. analyzed the effects of nanopore dimensions (pore diameter and pore length) and concluded that a smaller nanopore radius or a longer nanopore gives better ion selectivity.[27] Hsu et al. studied the effects of the shape of nanochannels on the RED performance by comparing

[1]College of Marine Engineering, Dalian Maritime University, Lingshui Road, Dalian 116026 China

[2]Dalian Key Lab of Marine Micro/Nano Energy and Self-Powered System, Dalian Maritime University, Dalian 116026, China

[3]Department of Information Science and Technology, Dalian Maritime University, Dalian 116026, China

[4]Liaoning Key Laboratory of Marine Sensing and Intelligent Detection, Dalian Maritime University, Dalian 116026, China

[5]These authors contributed equally

[6]Lead contact

*Correspondence: rpeng@dlmu.edu.cn (R.P.), xuminyi@dlmu.edu.cn (M.X.)

https://doi.org/10.1016/j.isci.2023.107184

bullet-shaped, conical-shaped, and flared nanochannels, and found that bullet-shaped nanochannels give the best power output values under the condition of similar channel diameter in the range of <1400 nm,[28] indicating that nanochannels with asymmetric structures which exhibit diode-like properties would give rise to superior RED performance in energy harvesting. As a result, it is reasonable to predict that a high-performance ionic diode would result in outstanding RED energy conversion efficiency.

Ionic diodes inspired by biological ion channels are categorized into two main branches, unipolar ionic diodes and bipolar ionic diodes, depending on the charge polarity of the ion-selective nanochannels,[29] which have been applied in constructing biosensors and electronics.[30,31] Many studies have proved that bipolar ionic diodes constructed with asymmetric charge density on the channel surface work better in terms of ion transport control compared to that of unipolar ionic diodes which have only one sign of electric charge on the channel surface.[32–34] For example, the difference in rectification characteristics between a bipolar ionic diode and a unipolar ionic diode based on a single conical nanochannel was studied by Gael Nguyen et al., and the result shows that the bipolar ionic diode can produce a better rectification effect than the unipolar diode when the surface charge density is similar.[35] To the best of our knowledge, most reported RED energy harvesting systems are developed based on unipolar ion-selective channels. Recent studies show that bipolar ionic diode systems have outstanding performance in RED energy conversion.[20,36–39] For example, an ionic diode membrane prepared by the combination of negatively charged mesoporous and positively charged carbon alumina nanopores is able to produce power densities of up to 3.46 W/m^2[40]; the nanochannel network combined by 1D and 3D nanochannels also shows ultrahigh osmotic energy conversion performance[41,42]; and a gel-based charged 3D network can produce power as high as 7.87 W/m^2 which has reached the benchmark for industrial requirements.[43] Although theoretical and numerical studies of ion transport through bipolar nanochannels for reverse osmosis energy collection and optimization have been reported previously.[33,44,45] However, the mechanism of boosting RED energy conversion performance by bipolar ionic diodes has not been symmetrically explored and extensive study of bipolar ionic diodes for the design and optimization of high-performance salinity energy harvester is needed to further optimize the RED system.

This work aims to provide insight into the working mechanism of RED energy harvesting by bipolar ionic diodes. RED voltage and power output of nanochannel-based ionic diodes under the conditions of various nanochannel properties, ionic solutions, and charging setups are numerically investigated by coupling the Poisson-Nernst-Planck and the Navier-Stokes equations. The energy conversion performance of the bipolar ionic diode-based RED system is extensively investigated. The results are compared with those of the unipolar ionic diodes-based RED system. A guideline for the design and optimization of a high-performance salinity energy harvester by tuning the working parameters of the bipolar ionic diodes including salt valence, ion strength, nanochannel size, and surface charge properties is provided. The results would also light up a new avenue for the applications of ionic diode systems, such as for seawater desalination.

Methods and numerical setup

Physical modeling

A numerical study of the steady-state RED process in a single straight nanochannel-based ionic diode was carried out using the finite element analysis (FEA) method, and unipolar ion-selective nanochannels without ionic diode layout were also calculated to understand the superiority of bipolar ionic diodes in salinity gradient energy harvesting. Figure 1A shows a schematic diagram of the bipolar ionic diode-based RED system, and Figure 1B shows the computational boundary conditions and geometric structures in the centrosymmetric view where a nanochannel of L in length and D in diameter is sandwiched by two reservoirs of L_r in length and D_r in diameter. To construct a typical bipolar ionic diode, the surface charge densities on the upstream and downstream sections of the nanochannel of 1/2 L in length are σ_1, σ_2, respectively. The upstream reservoir contains high concentration electrolyte solution of c_H and the downstream reservoir is filled with low concentration electrolyte solution of c_L ($c_H > c_L$), so that a concentration gradient can be created along the nanochannel and gives a RED electric potential.

Governing equations

The electric field in the computational domain where generally overlapping electric double layer (EDL) and selective ion transport happens can be determined by Poisson's equation[46]:

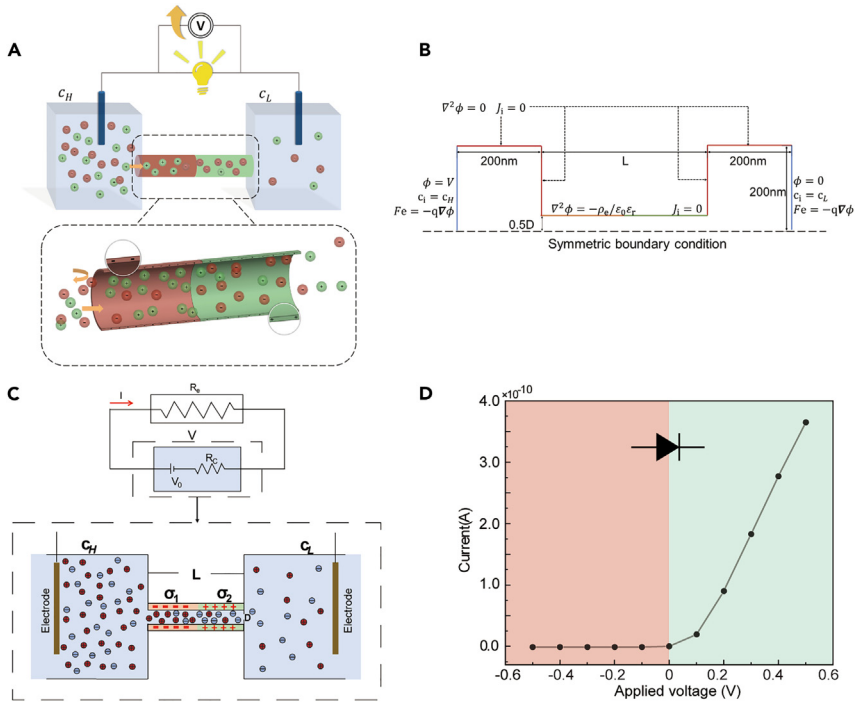

Figure 1. Modeling of the bipolar ionic diode-based RED system

(A) Schematic diagram and (B) the computational domain of the numerical modeling; (C) equivalent electric circuit of the bipolar ionic diode-based RED system; (D) Typical I-V curve of the bipolar ionic diode.

$$\nabla^2\varphi = -\frac{\rho_e}{\varepsilon_0\varepsilon_r} \quad \text{(Equation 1)}$$

$$\rho_e = F\sum z_i c_i \quad \text{(Equation 2)}$$

where ε_0 and ε_r are the vacuum dielectric constant and relative dielectric constant of the electrolyte medium, ρ_e and φ are the net charge density and electric potential, c_i, z_i are the molar concentration and valence of i^{th} ion, respectively, and F is the Faraday constant.

Transport of the i^{th} ion specie in the nanochannel driven by diffusion, migration, and convection which observes the conversion of ions can be calculated by the Nernst-Planck (NP) equation:

$$J_i = uc_i - D_i\nabla c_i - D_i\frac{Fz_i c_i}{RT}\nabla\varphi \quad \text{(Equation 3)}$$

$$\nabla J_i = 0 \quad \text{(Equation 4)}$$

where J_i and D_i are the flux and diffusion coefficient of i^{th} ion, $\boldsymbol{u}$ is the flow velocity, R is the gas constant. Note that net charge distribution near a charged channel surface because of the attraction of counterions and repulsion of co-ions builds up the EDL, and the thickness of EDL λ_D highly affects the effectiveness of ion transport behavior in the nanochannel which can be calculated by the Debye length κ_d[47],

$$\lambda_D = \frac{1}{\kappa_d} = \sqrt{\frac{\varepsilon_0\varepsilon_r RT}{F^2\sum c_i z_i^2}} \quad \text{(Equation 5)}$$

For a symmetrical electrolyte solution, λ_D can be simplified as $\lambda_D = \frac{3.04}{z_i\sqrt{M}} \times 10^{-10}(m)$, here M is the molarity of the ionic solution. Coordination of the thickness of EDL and the channel size is the key to ion transport control in a nanofluidic system.

For nanochannels with a size scale larger than 2 nm, continuous dynamics can be applied.[48] As a result, the flow field can be modeled by solving the steady-state Navier-Stokes equations. The contribution of the inertia term is negligible as microgeometry is used here; as a result, the flow field observes conservation of mass can be calculated by the following equations:

$$-\nabla p+\mu\nabla^2 \boldsymbol{u}+\boldsymbol{F}_e=0 \quad \text{(Equation 6)}$$

$$\nabla \boldsymbol{u}=0 \quad \text{(Equation 7)}$$

where μ is the coefficient of fluid viscosity, p is the pressure, and $\boldsymbol{F}_e$ is the volume force caused by electrostatic interactions because of the presence of the electric field and the net charges, which can be calculated by

$$\boldsymbol{F}_e=-F\sum z_i c_i \nabla\varphi \quad \text{(Equation 8)}$$

The boundary conditions are solved numerically by the equations presented in Figure 1B. Briefly, for the electric field, the surface charge density on the upstream and downstream of the channel wall is σ_1, and σ_2 respectively, and zero charge condition ($\boldsymbol{n}\cdot\nabla\varphi=0$) is applied on the walls of the channel reservoirs, where $\boldsymbol{n}$ denotes the component perpendicular to the channel wall. Here, the surface charge densities are assumed as constants to keep the problem simple, although the surface charge density may vary slightly depending on many factors such as pore size and concentration in reality.[49]

To solve for the distribution of both cations and anions, ion concentrations of c_H and c_L are applied on the entrance and exit of channel reservoirs, and a non-flux condition is applied on all channel surfaces ($\boldsymbol{n}\cdot D_i\nabla c_i=0$). For the flow field, a non-slip boundary condition and a no-permeation boundary condition ($\boldsymbol{u}=0$) are applied on the channel surfaces and reservoir surfaces, and zero pressure ($p=0$) is applied on the entrance and exit of the channel reservoirs. More details about the modeling and parameter setting can be found in the Supplementary Information (SI-1).

To calculate the electric voltage output of the bipolar ionic diode-based RED device, the RED system was modeled as an electric cell (see Figure 1C for the equivalent circuit), i.e., the upstream end of the bipolar ionic diode was applied with an electric potential, $\varphi=V$, and the downstream end of the cell was grounded, $\varphi=0$. Here V is associated with the operating voltage of the RED, with a net ionic flux (J_i) because of diffusion, electromigration, and convection, and the net charge flux gives the electric current (I) through

$$I=\int F\sum z_i c_i dA \quad \text{(Equation 9)}$$

where A is the cross-section area of the nanochannel. As a cell, an $I-V$ relationship can be obtained by varying the voltage, and open circuit voltage (OCV), internal resistance, and power output of the cell can be evaluated by the $I-V$, as explained below.

Data processing

The simulated bipolar ionic diode RED cell with an OCV of V_0 and internal resistance of R_C, is connected to an external resistor (R_e). An output voltage V is produced by the cell and a current of I is generated in the system, as shown in the equivalent circuit demonstrated in Figure 1C. One can easily get the following equation based on Kirchhoff's law:

$$V=V_0-IR_C \quad \text{(Equation 10)}$$

On the other hand, the operating voltage V can be calculated by using the external load R_e and the electric current of the circuit is as follows:

$$V=IR_e \quad \text{(Equation 11)}$$

According to Equation 10, the maximum output voltage of the RED, when no external current I is present, is V_0. In the simulation, we obtained the $I-V$ characteristics of the RED by using Equation 10. Specifically, by using different values of the operating voltage V we obtained values of I, and a curve fitting of the least square residual was performed. As a consequence, the corresponding OCV, V_0, and nano-channel resistance, R_C, can be calculated from the y-intercept and slope of the best linear fit (see SI-2 for an example of the processing details). The power output of the RED system can be simply expressed as:

$$P=IV \quad \text{(Equation 12)}$$

Apparently, when the output voltage becomes half of the maximum voltage (OCV) generated by the nanochannel ($V = 0.5V_0$), the power generation reaches its max value:

$$P_{max} = \frac{V_0^2}{4R_C} \quad \text{(Equation 13)}$$

where the subscript *max* indicates the conditions for maximum power generation. In this work, the maximum output power P_{max} and the correlated maximum output voltage were calculated for both bipolar ionic diode-based nanochannels and unipolar ion-selective nanochannels.

The numerical study was implemented by the FEA method with COMSOL Multiphysics (version 5.6), and a mesh-independent study was conducted (see SI-3 for more information). The working parameters of the RED system were extensively investigated based on a basic model. Unless otherwise specified, nanochannel size of 100 nm long and 10 nm in diameter, sodium chloride (NaCl) solutions of c_H = 10 mM and c_L = 0.1 mM, and surface charge densities of $\sigma_1 = -0.06\ C/m^2$, $\sigma_2 = 0.06\ C/m^2$ were applied. The effects of ion concentration, ion valence, channel length, channel diameter, surface charge density, and the symmetricity of charge polarity on the maximum output voltage and the maximum output power P_{max} produced by the RED system were investigated. Figure 1D shows a typical *I-V* characteristic of the basic model working under the condition of − 0.5–0.5 V range, in which one can see that the bipolar ionic diode-based nanochannel gives a typical "diode" performance, i.e., the ionic current is enhanced when a forward electric field is applied while the ionic current is depressed when a reversed electric field is applied, suggesting the excellent performance of nanochannel-based ionic diode in the respect of ion transport control.

RESULTS AND DISCUSSION

Channel size effect

The coordination of nanochannel pore size and the thickness of EDL dominates the selectivity of ion transport in a nanochannel, and the channel length determines the permeability of a nanochannel. A trade-off between ion selectivity and ion permeability is essential for constructing a high-performance RED system. For instance, nanochannels with a smaller pore size can give a higher ion selectivity intuitively[50]; however, a too-small channel pore size reduces the ion flux because of the reduction of internal space, thus bringing down the RED output performance.[51] Also, a longer charged nanochannel would enhance the repulsive effect of co-ions and give rise to a higher ion selectivity thus a better RED performance; however, on the other hand, when the channel is too long, diffusion resistivity increases dramatically and lowers the permeability, which results in a low RED output.[6]

In this section, the channel length effect and channel pore size effect on the performance of both unipolar and bipolar ionic diode-based RED systems under the same working fluids condition are presented. To shed light on the channel length effect, channel length in the range of 10~200 nm and channel pore size of 5 nm, 10 nm, and 20 nm under the condition of low c_H (10 mM) were simulated. The output voltages are demonstrated in Figures 2A–2C and the corresponding output powers are presented in Figures 2E and 2F. Channel length effect under the condition of high feeding concentration of c_H (500 mM) was also investigated, and the output voltage and output power are demonstrated in Figures 2G and 2H, respectively. To further investigate the pore size effect on the RED performance, channel pore diameter in the range of 2~20 nm working at the same channel length of 100 nm was calculated (Figure 2I).

From Figures 2A–2C one can see that the output voltage of all the bipolar cases is much higher than that of the unipolar ones, suggesting more excellent performance of bipolar ionic diode-based RED system compared to the unipolar counterpart in terms of voltage output. It is also obvious that for the bipolar cases, the output voltage increases with channel length and then decreases as the channel length increases further, indicating that there is a specific *L* where the curve reaches a plateau that maximizes the output voltage. The increase-decrease profile is caused by increasing ion selectivity of short channels and decreasing ion permeability thus increasing channel resistance of long channels as mentioned above, which has also been experimentally verified by Su et al.[52] As for the output power, from Figures 2D–2F one can get a general conclusion that the output power decreases with the channel length for both the unipolar and bipolar cases regardless of the channel diameter. The decreasing output power with increasing channel length is caused by the increasing internal resistance of the nanochannels with the channel length.

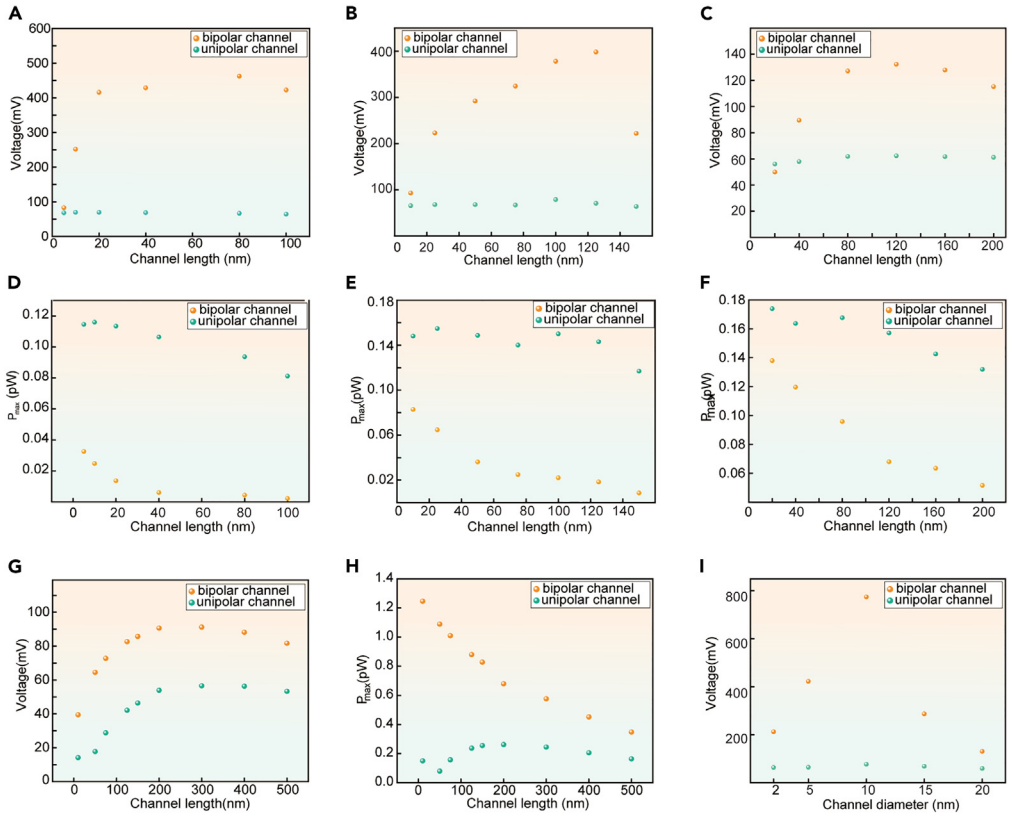

Figure 2. Channel size effect on the output performance of RED systems

Channel length effect on the output voltage of both unipolar and bipolar ionic diode-based RED systems working under the condition of different diameters of (A) 5 nm, (B) 10 nm, and (C) 20 nm; Channel length effect on the output power of both unipolar and bipolar ionic diode-based RED systems working under the condition of different diameter of (D) 5 nm, (E) 10 nm and (F) 20 nm; Channel length effect on the (G) output voltage and (H) output power of both unipolar and bipolar RED systems under the condition of high c_H (500 mM); (I) Channel diameter effect on the output voltage of both unipolar and bipolar RED systems where the channel length is 100 nm.

As the concentration of the feeding solution c_H increases to 500 mM, EDL gets weakly overlapped but the channel length effect on the performance of RED systems behaves very similarly compared to that of the low c_H (10 mM) case, for example, as shown in Figures 2G and 2H, there are optimum channel lengths to obtain maximum output voltage for both the unipolar case and the bipolar case, and for the bipolar case, the optimum output power decreases with increasing channel length. However, the output power of the unipolar case shows an optimum value at ~200 nm channel length which may be because of the tradeoff of channel resistance and the polarization of ions. It is worth noting that both the output voltage and output power of the bipolar cases are higher than those of the unipolar cases, suggesting the more excellent performance of the bipolar system than the unipolar counterpart in RED energy harvesting under the condition of high-concentration feeding solution. More discussions about the role of ion concentration in RED conversion are demonstrated in the following section.

In terms of the channel diameter effect on the performance of the RED system, in both the unipolar and bipolar cases, the output voltage shows an increasing and then decreasing trend as the channel diameter increases (Figure 2I), which can be explained by the tradeoff of high ion selectivity of small channels and low net charge current in large channels associated with the overlap of EDL.[53] For instance, for the bipolar case, the output voltage increases from ~200 mV to ~760 mV when the channel diameter increases from 2 nm to 10 nm, and this value decreases sharply to ~120 mV as the channel diameter increases to 20 nm. Apparently, when the channel diameter is very small, say 2 nm, EDL of 3 nm in thickness gets overlapped heavily in the channel ($2\lambda_D > D$), the channel becomes an ideal cation-selective tunnel (with respect to the charge polarity of the upstream nanochannel) and gives high ion selective effects in the channel; however, the

small aperture size results in a very low ion flux through the channel and therefore gives a low voltage output. On the other hand, when the channel diameter is too large, say 20nm, the large pore size increases the ion flux dramatically, but the EDL is too thin to get overlapped in such a large channel ($2\lambda_D > D$) thus cannot provide effective ion-selective transport; as a result, diffusion flux of co-ions weakens the net charge current and lowers the voltage output. Choosing the right channel size is therefore essential to maximize the energy harvesting performance of RED. Based on the simulation results demonstrated in Figure 2I one can see that the optimum channel diameter for both the unipolar case and the bipolar case is around 10nm, under which condition EDL gets overlapped ($2\lambda_D \approx D$), and ion selectivity and net charge flux of the RED system reaches an optimum condition.

An optimized channel size for a RED system always involves the combination of channel length and channel diameter. Figures 2A–2C presents the output voltage of the RED system working with different channel diameters of 5 nm, 10 nm, and 20 nm, it is obvious that for the bipolar case, the optimum channel length increases with channel pore size, for example, from ~60 nm to ~120 nm when the channel diameter increases from 5 to 20 nm. The optimum length for the unipolar case is not so prominent because of the overall low voltage output of the unipolar RED system which will be explained in the following section. To find an optimization route for the unipolar nanochannel RED system, an equation to estimate the optimum channel length has been reported.[16] Herein, it is hard to find a corresponding equation, but from the data, we can get a general conclusion that for the 10 mM/0.1 mM cases, a shorter channel length is more accessible to a higher output power; however, there is an optimum length to achieve maximum output voltage associate to the tradeoff of the ion selectivity and permeability. One can get a similar conclusion for the 500 mM/0.1 mM cases, i.e., an optimum channel length of ~200 nm is beneficial to the output voltage for both the unipolar cases and the bipolar cases, and a shorter channel length gives a better output power performance of the bipolar system. As a result, one can get a guideline for the optimization of a bipolar RED system with fixed pore size: (i) to obtain the optimized output voltage by using the numerical modeling and (ii) to enhance the output power by minimizing the channel length.

Besides the channel size effect, surprisingly, the voltage output of the bipolar RED cases is much higher than those of the unipolar counterpart (Figure 2I), proving our speculation that a bipolar ionic diode with excellent ion transport modulation is more suitable for high-performance RED system development. We believe that the outstanding performance results from the "one-way" transport behavior of bipolar ionic diodes. The mechanism is as follows: when counterions transport through a unipolar nanochannel with effective ion selectivity, a net charge flux builds up in the nanochannel and gives an output voltage; however, the counterions are likely to accumulate at the exit of the nanochannel because of the attraction force between the counters and the charged channel surface, which reduces the concentration gradient along the channel and gives a limited RED output. However, for the bipolar case, counterions get into the upstream channel driven by chemical potential and then pass through the downstream channel where the counterions become co-ions with respect to the downstream channel; as a result, charge carriers are repelled and move away from the exit of the nanochannel, which in turn increases the concentration gradient along the nanochannel and provides an effective charge transport efficiency and a high output performance.

Surface charge properties

As mentioned above, ionic diode-based nanochannels modified with asymmetric charges on the channel surface are excellent tunnels for ion manipulation (Figure 1C). The non-ohmic behavior of the diode characteristic effectively suppresses reverse currents, making ions move preferentially in one direction, which in turn effectively increases the output voltage of RED.[54] The performance of the ionic diode is dominated by the surface charge properties, including surface charge density, charge uniformity, charging length, and symmetricity of the nanochannel.[30] In this section, the effect of surface charge properties of nanochannels on the performance of the RED system was investigated by varying both the polarity and magnitude of surface charge densities as well as the length of charge surfaces based on the basic model.

To study the polarity of charge effect on the RED performance, the surface charge on the upstream of the nanochannel was set as constant, $\sigma_1 = -0.06\,C/m^2$, whereas the surface charge density at the downstream side (σ_2) sweeps in the range of $-0.09 \sim 0.09\,C/m^2$. Note that to fully understand the surface charge density effect under different ion strength conditions, both low-concentration $c_H = 10$ mM ($\lambda_D \approx 3\,nm$) (Figures 3A and 3B), and high-concentration $c_H = 500$ mM ($\lambda_D \approx 0.4\,nm$) (Figures 3C and 3D) feeding solutions were investigated.

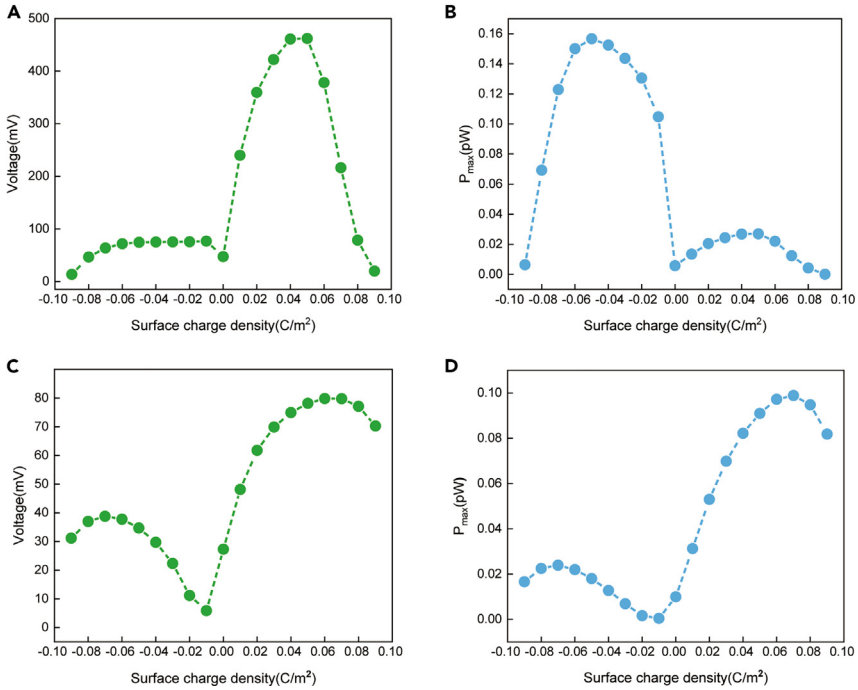

Figure 3. Surface charge effect on the performance of the ionic diode-based RED energy conversion

Surface charge density effect on the (A) output voltage and (B) maximum output power of ionic diode-based RED system under the condition of low-concentration feeding solution of c_H = 10 mM. Surface charge density effect on the (C) output voltage and (D) maximum output power of ionic diode-based RED system under the condition of high-concentration feeding solution of c_H = 500 mM. For all the cases, the concentration of NaCl on the downstream side is 0.1 mM.

From Figures 3A and 3B one can see that under the condition of 10 mM feeding solution, i.e., moderate overlapping of EDL in the nanochannel, when the surface charge on the downstream of the nanochannel is negative (which is the same sign as the upstream of the nanochannel), the nanochannel is a unipolar ion-selective channel, the output voltage is stable at around 90 mV; however, when the surface charge density on the downstream side becomes positive, the nanochannel becomes a bipolar ionic diode, the output voltage rises sharply with increasing surface charge density, peaking at $\sigma_2 \approx 0.05\ C/m^2$, and the output voltage drops as σ_2 increases further (Figure 3A). On the other hand, in terms of output power, for both the unipolar case and the bipolar case, the output power experiences an increase-decrease profile and maximizes at $-0.05\ C/m^2$ and $0.05\ C/m^2$ for the unipolar and bipolar cases respectively, which indicates that a highly uniform unipolar channel or a highly asymmetric bipolar channel would give rise to a high power output of the RED system.

For the case of weakly overlapping EDL in which high concentration c_H (500 mM, the concentration of ions in natural seawater) was applied, the voltage output (Figure 3C) and power output (Figure 3D) of both the unipolar case and the bipolar case show an increase-decrease profile, which again indicates that there is an optimum surface charge density value for the optimization of the bipolar ionic diode RED system. However, the optimum charge density on the downstream channel σ_2 shifts off a little bit from the highly uniform or asymmetric position ($-0.05\ C/m^2$ and $0.05\ C/m^2$), showing that regardless of the concentration of working fluids, a highly uniform unipolar channel or a highly symmetric bipolar channel is essential to the optimization of a RED system.

It is worth noting that for both the moderate and weak overlapping EDL cases, the optimum output voltage of the bipolar case is higher than that of the unipolar case (Figures 3A and 3C). For example, under the condition of $c_H = 10\ mM$, the optimum output voltage of the bipolar case is ~480 mV, which is ~6 times higher than that of the unipolar case, whereas under the condition of $c_H = 500\ mM$, the optimum output voltage of the bipolar case is only 80 mV but still ~2 times higher than that of the unipolar case, indicating a better voltage output performance of bipolar systems than unipolar ones under the conditions of both moderate and weak

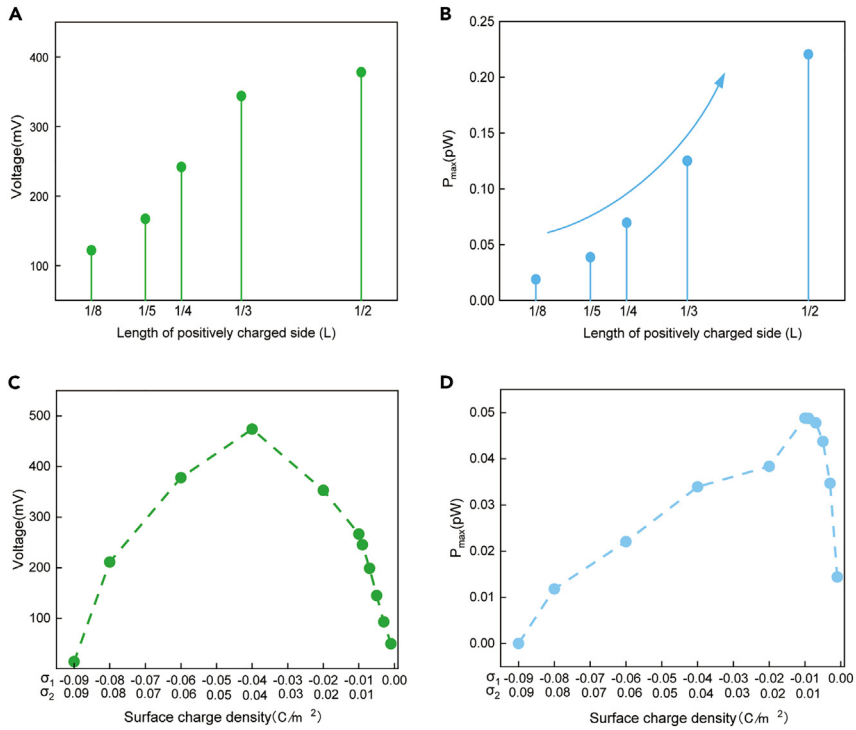

Figure 4. Charge polarity and charge magnitude effects on the performance of RED systems

Charge length layout effect on the (A) optimum output voltage and (B) maximum output power of the bipolar RED system. Charge magnitude effects on the (C) optimum output voltage and (D) maximum output power of bipolar RED systems.

EDL overlapping. However, regarding the optimum output power, under the condition of $c_H = 10mM$, the optimum output power of the bipolar case is ~0.02 pW which is only ~1/8 of the unipolar counterpart (~0.16 pW) (Figure 3B), whereas when c_H increases to 500 *mM*, the optimum output power of the bipolar case is ~0.1 pW, which is ~5 times higher than the unipolar case (Figure 3D).

The excellent output voltage performance is caused by ion enrichment at the unipolar channel exit and ion dissipation at the bipolar channel exit as mentioned above. The low optimum output power of the bipolar system working at low c_H is because of the higher resistance of the channel caused by the dissipation of ions at the channel exit and the related polarization behavior, whereas the high optimum power output of the bipolar system working at high c_H is caused by the superior diode-like transport property of the bipolar vsystem. As can be seen, the optimum output power of both the bipolar and unipolar cases is highly affected by the interplay of charge polarization and ion-selective transport in nanofluidic systems resulting from ion properties. Discussions about the concentration and valence of ions on the RED performance will be presented in the following section.

Based on the above-mentioned conclusion, we further investigated the charge length and charge magnitude effects on the performance of the RED system (Figure 4). Asymmetric charge modification length by varying the length of the positively charged downstream section (L_{down}) from 1/8 *L* to 1/2 *L* while remaining the upstream section (L_{up}) negatively charged ($L_{up} = L - L_{down}$). Figures 4A and 4B show the results of the length effect on the optimum output voltage and the optimum output power of the bipolar system. From Figure 4A one can see that the optimum output voltage increases from ~150 mV to ~750 mV and the optimum output power increases from ~0.02 pW to ~0.23 pW as the charging length of the positively charged side increases from 1/8 *L* to 1/2 *L*, indicating that a highly symmetric charging length layout is beneficial to the high performance of bipolar RED systems because of the effective modulation of net charge transport. In addition, highly symmetric bipolar RED systems under the conditions of $\sigma_1 = -\sigma_2$ (bipolar) in the range of $0 \sim -0.09\ C/m^2$ were also simulated to explore the effect of the charge density magnitude on the RED performance (see Figures 4C and 4D for the results). Apparently, for the bipolar case, the output voltage maximizes at ~0.055 C/m^2 and the output power maximum at ~0.01 C/m^2, which is

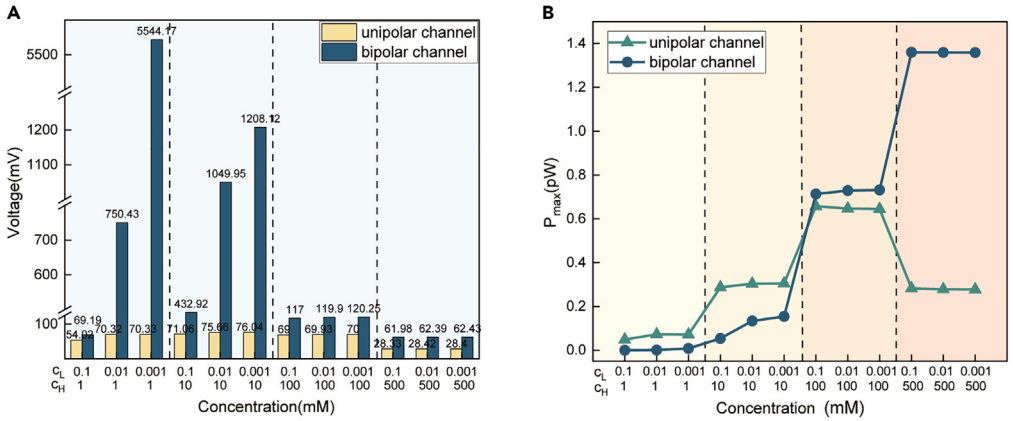

Figure 5. Concentration effect on the performance of both unipolar and bipolar RED systems

Concentration effect on (A) the optimum output voltage and (B) maximum output power working with different concentration combinations, in which the channel is 50 nm in length and 10 nm in diameter, and c_L of 0.1, 0.01, 0.001 mM and c_L from 1 mM to 500 mM are applied.

different from those of the unipolar case where the output voltage maximizes at ~0.01 C/m^2 (Figure S3A), and the maximum output power decrease with the magnitude of the charge density (Figure S3B). It can be seen that an appropriate surface charge density is a fundamental requirement for achieving ion selectivity and satisfactory RED energy conversion performance, an excessive or insufficient surface charge can negatively affect the output performance of nanofluidic-based REDs.[55] The performance of the bipolar RED system is also affected by the symmetricity of charging length and charge magnitude of the upstream and downstream channels, and a highly symmetric bipolar ionic diode with a symmetric charging length of opposite sign would give rise to the high performance of the system under the condition of a suitable ionic environment.

Ion concentration

The thickness of EDL is a function of ion concentration and valence of the electrolyte (Equation 5), and the performance of RED is highly dependent on the effectiveness of ion selection caused by the overlapping of EDL. In this section, the ion concentration effect on the output voltage and output power of both bipolar and unipolar nanochannels were investigated by using different concentration combinations of c_H and c_L. To obtain comprehensive conclusions, three values of c_L, 0.1, 0.01 and 0.001 mM and four high-concentration values of c_H 1, 10, 100 and 500 mM were applied so that both high-concentration gradient and low-concentration gradient circumstances would be explored (Figure 5).

Figure 5A illustrates the concentration effects on the voltage output of both the unipolar and bipolar RED systems. From Figure 5A one can get three key findings: (i) The output voltage of the bipolar cases is much higher than those of the unipolar ones when the same concentration gradient is applied, especially under the condition of low concentration of c_H, 10mM ($\lambda_D \approx 3nm$) and 1mM ($\lambda_D \approx 10nm$), in which moderate and heavy overlapping of EDL happens in the nanochannels; (ii) under the condition of a fixed c_H, the output voltage of both the unipolar cases and the bipolar cases increases as c_L decreases from 0.1mM to 0.001 mM, indicating that a higher concentration gradient is beneficial to the high output voltage; (iii) under the condition of a fixed c_L, the output voltage of both the unipolar cases and the bipolar cases experiences an "increase-decrease" profile as c_H increases from 1 mM to 500 mM, except for the bipolar case working at c_L = 0.001 mM in which the output voltage of the bipolar case decreases continuously as c_H increases. The results prove that the choosing of c_H is critical to the optimization of the voltage output of the RED system.

The outstanding performance of the bipolar RED system in terms of output voltage working under the condition of 0.001 mM/1 mM is assumed caused by the reduction of ion concentration polarization in nanochannels. Figure S4 compares the concentration distribution inside the channel working under the conditions of (a) c_H = 1 mM and c_L = 0.001 mM and (b) c_H = 1 mM and c_L = 0.01 mM. It can be seen that when c_L = 0.001 mM, the ion concentration polarization (ICP) effect of the channel is significantly weakened, and the reduced ICP is beneficial to the permeability and ion selectivity of the nanochannel.[56] In addition, the

lower c_L would give rise to a higher concentration gradient which would further enhance the output voltage. The "increase-crease" trend of the other cases is assumed because of the trade-off of the concentration gradient and the ICP effect.

The concentration effect on the power output of both the unipolar and bipolar RED systems is presented in Figure 5B, from which one can also get three key conclusions: (i) The output power of the bipolar cases is lower than those of the unipolar ones when c_H is lower than 10 mM, and the output power of the bipolar cases is higher than those of the unipolar ones when c_H is higher than 100 mM, which shows that the unipolar system is more efficient when the concentration of feeding solution is low, and the bipolar system is more suitable for the cases when high-concentration feeding solution is applied; (ii) under the condition of a fixed c_H, the output voltage of both the unipolar cases and the bipolar cases changes very little as c_L increases from 0.1 mM to 0.001 mM, indicating that the concentration in of the downstream reservoir has a minor effect on the output power of RED systems and the maximum output power is dominated by the feeding concentration c_H; (iii) under the condition of a fixed c_L, the output power of the unipolar cases experiences an "increase-decrease" profile as c_H increases from 1 mM to 500 mM, which is consistent with the reported result,[27] whereas the output power of the bipolar cases increases dramatically as c_H increases from 1 mM to 500 mM, suggesting that the advantages of the bipolar structure in RED energy harvesting, especially under the condition of high-concentration feeding solution, such as natural seawater.

Based on the above-mentioned discussions, one can get the following routes to optimize the concentration of working fluids of RED systems. In terms of voltage output, a bipolar system gives higher voltage output than a unipolar system because of the outstanding performance of bipolar ionic diodes in counterion delivery and polarization elimination as mentioned above. The concentration gradient provides the driven chemical potential for the RED system. As a result, a higher concentration gradient would give rise to a higher diffusion net charge flux under the same channel system with the same ion selectivity thus a higher output voltage. However, overlapping of EDL in a nanochannel depends on the concentration of ions, i.e., as the concentration increases the ion selectivity of the nanochannel decreases, which in turn lowers the net charge flux and the output voltage for both unipolar and bipolar systems.[51] Therefore, enhancing the concentration gradient and meanwhile maintaining the ion selectivity of the nanochannel is the key to developing a high-output voltage RED system. However, to achieve higher optimum power output, when the concentration of the feeding solution is low, it is feasible to achieve high power output by using the unipolar system because of the relatively low resistance of the unipolar cell compared to the bipolar system; when the concentration of feeding solution is high, the bipolar system is able to rectify the net charge flux and gives rise to higher power output. As a result, the key to obtaining a high-power-output RED system is to enhance the concentration gradient and meanwhile maintain the efficiency of net charge flux in the nanochannel to minimize the internal resistance of the RED system.

Ion valence

Numerous monovalent and multivalent salt ions in natural seawater have different hydration radii, ionic diffusivity, charge numbers, etc., and all these factors have a significant impact on the output of the RED system.[57,58] For example, Song et al. investigated the influences of divalent ions on a unipolar RED system and found that multivalent ions affect the output of RED which is dependent on the polarity of nanochannels.[57,59] In this section, the effect of ion valence on the output performance of the bipolar RED system was studied by using typical cations and anions in natural seawater. Three monovalent cations, Li^+, Na^+, K^+, three divalent cations, Mg^{2+}, Cu^{2+}, Ca^{2+} and one typical trivalent cation, Al^{3+} of 10 mM were studied. To achieve a comprehensive understanding of the valence effect, monovalent anion Cl^- and divalent anion SO_4^{2-} were applied. The diffusion coefficient of Li^+, Na^+, K^+, Cl^-, SO_4^{2-}, Mg^{2+}, Cu^{2+}, $Ca^{2+}$and Al^{3+} at room temperature are 1.03×10^{-9}, 1.33×10^{-9}, 1.96×10^{-9}, 2.03×10^{-9}, 1.07×10^{-9}, 0.705×10^{-9},0.714×10^{-9},0.792×10^{-9}, and $0.541\times 10^{-9} m^2/s$, respectively.[60] The results are demonstrated in Figure 6.

Figure 6A shows the effect of the valence of cations (10 mM/0.1 mM) on the output voltage and maximum output power of the bipolar RED system. From Figure 6A one can see that the output voltages of the monovalent cation cases are higher than those of the multivalent cation cases, and the maximum output power increases with the valence of cations. For the monovalent cases, generally speaking, when a cation-selective nanochannel is applied, both the output voltage and output power show the trend of $Li^+<Na^+<K^+$ because cations with higher diffusion ecoefficiency give higher net-charge flux; i.e., $Li^+<Na^+<K^+$.[5] But for an anion-selective channel, anion (Cl^-) is the charge carrier and contribute the net charge current,

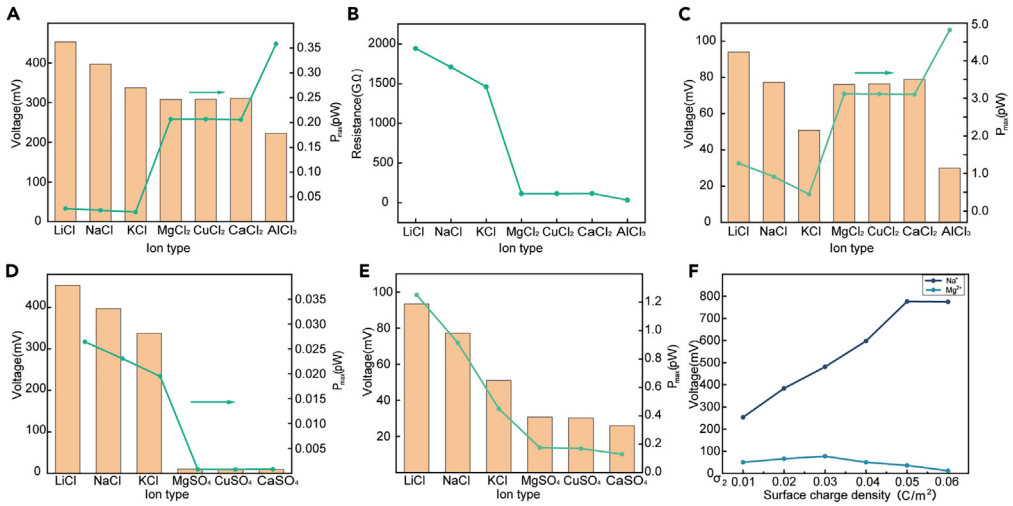

Figure 6. Ion valence effect on the performance of bipolar RED systems

(A) Effect of cation valence on the output voltage and maximum power of bipolar RED system under the condition of low concentration c_H (10 mM); (B) Internal resistance of bipolar RED system working with cations of different valence. (C) Effect of cation valence on the output voltage and maximum power of bipolar RED system under the condition of high concentration c_H (500 mM); Effect of multivalent anion on the output voltage and maximum power of bipolar RED system under the condition of (D) low concentration c_H (10 mM) and (E) high concentration c_H (500 mM); (F) Comparison of the output voltage of bipolar RED systems working with monovalent cation Na^+ and bivalent cation Mg^{2+} of 10 mM under different channel surface charge conditions.

cations with higher diffusion coefficient would enhance the diffusion flux of the cations, thus lowering the net charge flux and the output performance; thus, for an anion-selective channel, the output voltage, and the output power following the trend $Li^+>Na^+>K^+$.[5] As seen from the bipolar nanochannel demonstrated in Figure 6A, both the output voltage and output power of the monovalent cases show the trend $Li^+>Na^+>K^+$, which is consistent with the unipolar anion-selective channel mentioned above. As a consequence, we believe that the bipolar nanochannel system is an anion-selective channel, and Cl^- is the net charge carrier.

For the bivalent cases where Mg^{2+}, Cu^{2+}, and Ca^{2+} are applied, the output voltages are lower than those of the monovalent cases and the output powers are much higher than those of the monovalent cases. These trends can be explained as follows: On one hand, for the bipolar nanochannel system, bivalent cations are attracted by the negatively charged upstream nanochannel and screen the channel surface with thinner EDL, which allows more anions to penetrate into the nanochannel and gives rise to a higher diffusion flux of anions; however, on the other hand, as bivalent cations are applied, diffusion of bivalent cations with more charges through the downstream nanochannel will neutralize the anion flux thus decrease the total net charge flux compared to the monovalent cations. The trade-off of the enhancement of anions flux and higher flux of bivalent cations with more charges gives the lower output voltage compared to the monovalent cases. As a result, the decrease in the output voltage is more pronounced for the trivalent case where Al^{3+} is applied (Figure 6A).

The maximum output power of RED is associated with the output voltage and the internal resistance (R_C). For instance, the output voltage of the bivalent cation cases Mg^{2+}, Cu^{2+}, and Ca^{2+} is lower than those of the monovalent cation cases; however, the internal resistance of the bivalent cation cases is ~100 times lower than those of the monovalent cation cases (Figure 6B), which give rise to the high output power. The low internal resistance of the bivalent cation cases is attributed to the doubled concentration of anion Cl^- and the high valence of cations that carry more charges. The concentration distribution of monovalent and bivalent cations along the axis of the channel can be found in Figure S2 demonstrated in SI-4.

The output power is highly enhanced when triple valent cations are applied. For example, the output power of the $AlCl_3$ case (~0.36 pW) is much higher compared to the bivalent cation cases (~0.2 pW). We also calculated the corresponding RED output under the condition of a high concentration of c_H = 500 *mM*, and found that although high concentration feeding solution with thinker EDL would give rise to a higher

charge screening effect; however, the output voltage and the output power still follow the rules discussed above, but with lower output voltage and higher output power compared to those of the low c_H cases, as shown in Figure 6C. It can be seen that the selection of a suitable electrolyte solution is important for optimizing the output performance of the RED. The result is the ideal case of the effect of different valence ions on the output performance of the RED, but the real seawater is a mixture of multiple valence ions and its real situation will be more complex.[61]

We also investigated the effect of bivalent anion SO_4^{2-} on the output power and output voltage of the bipolar RED system by using symmetric electrolytes including Mg SO_4, Cu SO_4, Ca SO_4 of both high c_H of 500 mM and c_H of 10 mM (Figure 6D). From Figure 6D one can see that for both the high c_H and the low c_H cases, the output voltage and output power of the bivalent anion cases are much lower than those of the monovalent cases, and the decrement is more pronounced as c_H become lower. As mentioned above, the bipolar RED system is an overall anion-selective channel and anions are the net charge carriers. When SO_4^{2-} is applied, the net charge flux decreases dramatically because of the low diffusion coefficient of SO_4^{2-} compared to that of Cl^-, which results in a low output voltage. The pronounced decrement of output voltage and the output power of the bivalent cases is because of the prominent overlapping of EDL and charge screening effect of low c_H, which has also been reported in the literature.[58] As a consequence, it is essential to take both the cation valence and the anion valence into consideration during the optimization of the bipolar RED salinity energy conversion system.

Limitations of the study

Our results are subject to several limitations: (1) All the data obtained in this article are based on numerical simulations, it is necessary to further prove the conclusions of this study through experimental research and (2) only basic parameters are involved in the current model, synergistic effects of multiple parameters, such as wall slip and pH environment are not considered in this work.

Conclusions

Overall, this article investigates RED energy conversion by both unipolar and bipolar ion-selective nanochannels, and the effects of channel size, polarity and magnitude of charge surface, concentration, and valence of ionic solution on the maximum output voltage and maximum output power are symmetrically studied by numerical simulations, and a guideline for optimizing bipolar ionic diode-based RED energy conversion system is provided. The results show that there are optimum channel length-diameter combinations to achieve maximum output voltage for both unipolar and bipolar RED systems because of the trade-off of ion selectivity and permeability. Optimum output performance can be obtained on highly uniform unipolar nanochannel with uniform charges and highly symmetric bipolar ionic diode with an asymmetric surface charge of the same magnitude and length. The maximum output power can be increased by increasing the concentration gradient of the solution. For the bipolar RED system, multivalent cations would decrease the output voltage but would highly increase the maximum output power, whereas multivalent anions would decrease both the output voltage and the maximum output power. The results also prove that under the condition of a high-concentration feeding solution, the bipolar RED system has better performance than the unipolar RED system in terms of both maximum output voltage and maximum output power. This study not only provides quantitative results for RED output under different conditions but also provides a new idea for the structural optimization of the ion diode-based device for collecting salinity gradient energy in the future.

STAR★METHODS

Detailed methods are provided in the online version of this paper and include the following:

- KEY RESOURCES TABLE
- RESOURCE AVAILABILITY
  - Lead contact
  - Data and code availability
- METHOD DETAILS
  - Physical modeling
  - Data processing

SUPPLEMENTAL INFORMATION

Supplemental information can be found online at https://doi.org/10.1016/j.isci.2023.107184.

ACKNOWLEDGMENTS

The authors acknowledge funding support from the National Natural Science Foundation of China (83121063, 83122015), the Fundamental Research Funds for the Central Universities in China (3132022214) and Natural Science Foundation of Liaoning Province (2022-MS-156), and China Postdoctoral Science Foundation (2022MS720621).

AUTHOR CONTRIBUTIONS

R.P. generated the ideas, edited the manuscript; R.P. and T.L. conducted the simulation and wrote the daft of the manuscript, H.S. and S.W. organized the data and conducted the simulation, Y.S., J.W., R.P., and M.X. coordinated and supervised this project.

DECLARATION OF INTERESTS

The authors declare no conflict of interest.

INCLUSION AND DIVERSITY

We support inclusive, diverse, and equitable conduct of research.

Received: February 15, 2023
Revised: April 18, 2023
Accepted: June 16, 2023
Published: June 20, 2023

REFERENCES

1. Hussain, A., Arif, S.M., and Aslam, M. (2017). Emerging renewable and sustainable energy technologies: State of the art. Renew. Sustain. Energy Rev. *71*, 12–28. https://doi.org/10.1016/j.rser.2016.12.033.

2. Melikoglu, M. (2018). Current status and future of ocean energy sources: A global review. Ocean Eng *148*, 563–573. https://doi.org/10.1016/j.oceaneng.2017.11.045.

3. Borthwick, A.G. (2016). Marine Renewable Energy Seascape. Engineering *2*, 69–78. https://doi.org/10.1016/J.ENG.2016.01.011.

4. Lee, Y., Kim, H.J., and Kim, D.K. (2020). Power generation from concentration gradient by reverse electrodialysis in anisotropic nanoporous anodic aluminum oxide membranes. Energies *13*, 904. https://doi.org/10.3390/en13040904.

5. Cao, L., Guo, W., Ma, W., Wang, L., Xia, F., Wang, S., Wang, Y., Jiang, L., and Zhu, D. (2011). Towards understanding the nanofluidic reverse electrodialysis system: Well matched charge selectivity and ionic composition. Energy Environ. Sci. *4*, 2259–2266. https://doi.org/10.1039/c1ee01088c.

6. Chanda, S., and Tsai, P.A. (2019). Numerical simulation of renewable power generation using reverse electrodialysis. Energy *176*, 531–543. https://doi.org/10.1016/j.energy.2019.03.136.

7. Pakulski, D., Czepa, W., Buffa, S.D., Ciesielski, A., and Samorì, P. (2020). Atom-Thick Membranes for Water Purification and Blue Energy Harvesting. Adv. Funct. Mater. *30*, 1902394–1902421. https://doi.org/10.1002/adfm.201902394.

8. Jiao, Y., Song, L., Zhao, C., An, Y., Lu, W., He, B., and Yang, C. (2022). Membrane-based indirect power generation technologies for harvesting salinity gradient energy - A review. Desalination *525*, 115485. https://doi.org/10.1016/j.desal.2021.115485.

9. Tong, X., Liu, S., Crittenden, J., and Chen, Y. (2021). Nanofluidic Membranes to Address the Challenges of Salinity Gradient Power Harvesting. ACS Nano *15*, 5838–5860. https://doi.org/10.1021/acsnano.0c09513.

10. Zhou, Y., and Jiang, L. (2020). Bioinspired Nanoporous Membrane for Salinity Gradient Energy Harvesting. Joule *4*, 2244–2248. https://doi.org/10.1016/j.joule.2020.09.009.

11. Zhang, Z., Wen, L., and Jiang, L. (2021). Nanofluidics for osmotic energy conversion. Nat. Rev. Mater. *6*, 622–639. https://doi.org/10.1038/s41578-021-00300-4.

12. Pawlowski, S., Sistat, P., Crespo, J.G., and Velizarov, S. (2014). Mass transfer in reverse electrodialysis: Flow entrance effects and diffusion boundary layer thickness. J. Membr. Sci. *471*, 72–83. https://doi.org/10.1016/j.memsci.2014.07.075.

13. Kim, D.K., Duan, C., Chen, Y.F., and Majumdar, A. (2010). Power generation from concentration gradient by reverse electrodialysis in ion-selective nanochannels. Microfluid. Nanofluidics *9*, 1215–1224. https://doi.org/10.1007/s10404-010-0641-0.

14. Pattle, R.E. (1954). Production of electric power by mixing fresh and salt water in the hydroelectric pile. Nature *174*, 660.

15. Chein, R., and Liu, B. (2016). Energy conversion from electrolyte concentration gradient using charged nano-pores. Int. J. Green Energy *13*, 1400–1411. https://doi.org/10.1080/15435075.2016.1206900.

16. Kim, D.H., Phillips, M.E., Chang, A.Y., Patel, H.K., Nguyen, K.T., and Willhite, D.C. (2011). Numerical study of power generation by reverse electrodialysis. Front. Neural Circ. *5*, 5–10. https://doi.org/10.1007/s12206-010-1113-x.

17. Alizadeh, A., and Wang, M. (2018). Reverse electrodialysis through nanochannels with inhomogeneously charged surfaces and overlapped electric double layers. J. Colloid Interface Sci. *529*, 214–223. https://doi.org/10.1016/j.jcis.2018.05.111.

18. Kim, J., Jeon, J., Wang, C., Chang, G.T., and Park, J. (2022). Asymmetric Nanochannel Network-Based Bipolar Ionic Diode for Enhanced Heavy Metal Ion Detection. ACS Nano *16*, 8253–8263. https://doi.org/10.1021/acsnano.2c02016.

19. Wu, Z.-Q., Li, C.-Y., Ding, X.-L., Li, Z.-Q., and Xia, X.-H. (2022). Synergistic Effect of Electrostatic Interaction and Ionic Dehydration on Asymmetric Ion Transport in Nanochannel/Ion Channel Composite

Membrane. J. Phys. Chem. Lett. *13*, 5267–5274. https://doi.org/10.1021/acs.jpclett.2c01166.

20. Chen, L., Tu, B., Lu, X., Li, F., Jiang, L., Antonietti, M., and Xiao, K. (2021). Unidirectional ion transport in nanoporous carbon membranes with a hierarchical pore architecture. Nat. Commun. *12*, 4650–4657. https://doi.org/10.1038/s41467-021-24947-3.

21. Kwak, S.H., Kwon, S.R., Baek, S., Lim, S.M., Joo, Y.C., and Chung, T.D. (2016). Densely charged polyelectrolyte- stuffed nanochannel arrays for power generation from salinity gradient. Sci. Rep. *6*, 26416. https://doi.org/10.1038/srep26416.

22. Tong, X., Wang, X., Liu, S., Gao, H., Xu, C., Crittenden, J., and Chen, Y. (2018). A freestanding graphene oxide membrane for ef fi ciently harvesting salinity gradient power. Carbon N. Y. *138*, 410–418. https://doi.org/10.1016/j.carbon.2018.07.064.

23. Cheng, S.Q., Zhang, S.Y., Min, X.H., Tao, M.J., Han, X.L., Sun, Y., and Liu, Y. (2022). Photoresponsive Solid Nanochannels Membranes: Design and Applications. Small *18*, 21050199–e2105115. https://doi.org/10.1002/smll.202105019.

24. Sui, X., Zhang, Z., Li, C., Gao, L., Zhao, Y., Yang, L., Wen, L., and Jiang, L. (2019). Engineered Nanochannel Membranes with Diode-like Behavior for Energy Conversion over a Wide pH Range. ACS Appl. Mater. Interfaces *11*, 23815–23821. https://doi.org/10.1021/acsami.8b02578.

25. Li, J., Zhang, K., Zhao, X., and Li, D. (2022). Single Artificial Ion Channels with Tunable Ion Transport Based on the Surface Modification of pH-Responsive Polymers. ACS Appl. Mater. Interfaces *14*, 27130–27139. https://doi.org/10.1021/acsami.2c03949.

26. Ji, J., Kang, Q., Zhou, Y., Feng, Y., Chen, X., Yuan, J., Guo, W., Wei, Y., and Jiang, L. (2017). Osmotic Power Generation with Positively and Negatively Charged 2D Nanofluidic Membrane Pairs. Adv. Funct. Mater. *27*, 1603623–1603628. https://doi.org/10.1002/adfm.201603623.

27. Tseng, S., Li, Y.M., Lin, C.Y., and Hsu, J.P. (2016). Salinity gradient power: Influences of temperature and nanopore size. Nanoscale *8*, 2350–2357. https://doi.org/10.1039/c5nr07563g.

28. Hsu, J.P., Su, T.C., Lin, C.Y., and Tseng, S. (2019). Power generation from a pH-regulated nanochannel through reverse electrodialysis: Effects of nanochannel shape and non-uniform H+ distribution. Electrochim. Acta *294*, 84–92. https://doi.org/10.1016/j.electacta.2018.10.074.

29. Huang, X., Kong, X.Y., Wen, L., and Jiang, L. (2018). Bioinspired Ionic Diodes: From Unipolar to Bipolar. Adv. Funct. Mater. *28*, 1801079. https://doi.org/10.1002/adfm.201801079.

30. Peng, R., Pan, Y., Liu, B., Li, Z., Pan, P., Zhang, S., Qin, Z., Wheeler, A.R., Tang, X.S., and Liu, X. (2021). Understanding Carbon Nanotube-Based Ionic Diodes: Design and Mechanism. Small *17*, e2100383. https://doi.org/10.1002/smll.202100383.

31. Peng, R., Pan, Y., Li, Z., Zhang, S., Wheeler, A.R., Tang, X.S., and Liu, X. (2020). Ionotronics Based on Horizontally Aligned Carbon Nanotubes. Adv. Funct. Mater. *30*, 2003177. https://doi.org/10.1002/adfm.202003177.

32. Yan, F., Yao, L., Yang, Q., Chen, K., and Su, B. (2019). Ionic Current Rectification by Laminated Bipolar Silica Isoporous Membrane. Anal. Chem. *91*, 1227–1231. https://doi.org/10.1021/acs.analchem.8b04639.

33. Kalman, E.B., Sudre, O., Vlassiouk, I., and Siwy, Z.S. (2009). Control of ionic transport through gated single conical nanopores. Anal. Bioanal. Chem. *394*, 413–419. https://doi.org/10.1007/s00216-008-2545-3.

34. Vlassiouk, I., Kozel, T.R., and Siwy, Z.S. (2009). Biosensing with nanofluidic diodes. J. Am. Chem. Soc. *131*, 8211–8220. https://doi.org/10.1021/ja901120f.

35. Nguyen, G., Vlassiouk, I., and Siwy, Z.S. (2010). Comparison of bipolar and unipolar ionic diodes. Nanotechnology *21*, 265301. https://doi.org/10.1088/0957-4484/21/26/265301.

36. Wu, Y., Zhou, T., Wang, Y., Qian, Y., Chen, W., Zhu, C., Niu, B., Kong, X.Y., Zhao, Y., Lin, X., et al. (2022). The synergistic effect of space and surface charge on nanoconfined ion transport and nanofluidic energy harvesting. Nano Energy *92*, 106709. https://doi.org/10.1016/j.nanoen.2021.106709.

37. Zhang, Z., Kong, X.Y., Xiao, K., Liu, Q., Xie, G., Li, P., Ma, J., Tian, Y., Wen, L., and Jiang, L. (2015). Engineered Asymmetric Heterogeneous Membrane: A Concentration-Gradient-Driven Energy Harvesting Device. J. Am. Chem. Soc. *137*, 14765–14772. https://doi.org/10.1021/jacs.5b09918.

38. Chen, W., Xiang, Y., Kong, X.Y., and Wen, L. (2022). Polymer-based membranes for promoting osmotic energy conversion. Giant *10*, 100094. https://doi.org/10.1016/j.giant.2022.100094.

39. Hou, S., Zhang, Q., Zhang, Z., Kong, X., Lu, B., Wen, L., and Jiang, L. (2021). Nano Energy Charged porous asymmetric membrane for enhancing salinity gradient energy conversion. Nano Energy *79*, 105509. https://doi.org/10.1016/j.nanoen.2020.105509.

40. Gao, J., Guo, W., Feng, D., Wang, H., Zhao, D., and Jiang, L. (2014). High-performance ionic diode membrane for salinity gradient power generation. J. Am. Chem. Soc. *136*, 12265–12272. https://doi.org/10.1021/ja503692z.

41. Li, C., Wen, L., Sui, X., Cheng, Y., Gao, L., and Jiang, L. (2021). Large-scale, robust mushroom-shaped nanochannel array membrane for ultrahigh osmotic energy conversion. Sci. Adv. *7*, eabg2183–8. https://doi.org/10.1126/sciadv.abg2183.

42. Chen, W., Wang, Q., Chen, J., Zhang, Q., Zhao, X., Qian, Y., Zhu, C., Yang, L., Zhao, Y., Kong, X.Y., et al. (2020). Improved Ion Transport and High Energy Conversion through Hydrogel Membrane with 3D Interconnected Nanopores. Nano Lett. *20*, 5705–5713. https://doi.org/10.1021/acs.nanolett.0c01087.

43. Bian, G., Pan, N., Luan, Z., Sui, X., Fan, W., Xia, Y., Sui, K., and Jiang, L. (2021). Anti-Swelling Gradient Polyelectrolyte Hydrogel Membranes as High-Performance Osmotic Energy Generators. Angew. Chem. *133*, 20456–20462. https://doi.org/10.1002/ange.202108549.

44. Picallo, C.B., Gravelle, S., Joly, L., Charlaix, E., and Bocquet, L. (2013). Nanofluidic osmotic diodes: Theory and molecular dynamics simulations. Phys. Rev. Lett. *111*, 244501–244505. https://doi.org/10.1103/PhysRevLett.111.244501.

45. Li, C., Liu, P., Zhai, Y., Yao, L., Lin, H., Gao, L., and Jiang, L. (2022). Unconventional Dual Ion Selectivity Determined by the Forward Side of a Bipolar Channel toward Ion Flux. ACS Appl. Mater. Interfaces *14*, 2230–2236. https://doi.org/10.1021/acsami.1c18474.

46. Li, D. (2004). Electrokinetics in Microfluidics (Academic Press).

47. Hunter, R.J. (1981). Zeta Potential in Colloid Science: Principles and Applications (Academic press).

48. Peng, R., and Li, D. (2016). Electroosmotic flow in single PDMS nanochannels. Nanoscale *8*, 12237–12246. https://doi.org/10.1039/C6NR02937J.

49. Kang, B.D., Kim, H.J., Lee, M.G., and Kim, D.K. (2015). Numerical study on energy harvesting from concentration gradient by reverse electrodialysis in anodic alumina nanopores. Energy *86*, 525–538. https://doi.org/10.1016/j.energy.2015.04.056.

50. Zerafat, M.M., Shariati-Niassar, M., Hashemi, S.J., Sabbaghi, S., Ismail, A.F., and Matsuura, T. (2013). Mathematical modeling of nanofiltration for concentrated electrolyte solutions. Desalination *320*, 17–23. https://doi.org/10.1016/j.desal.2013.04.015.

51. Laucirica, G., Albesa, A.G., Toimil-Molares, M.E., Trautmann, C., Marmisollé, W.A., and Azzaroni, O. (2020). Shape matters: Enhanced osmotic energy harvesting in bullet-shaped nanochannels. Nano Energy *71*, 104612–104618. https://doi.org/10.1016/j.nanoen.2020.104612.

52. Hsu, J.P., Su, T.C., Peng, P.H., Hsu, S.C., Zheng, M.J., and Yeh, L.H. (2019). Unraveling the Anomalous Surface-Charge-Dependent Osmotic Power Using a Single Funnel-Shaped Nanochannel. ACS Nano *13*, 13374–13381. https://doi.org/10.1021/acsnano.9b06774.

53. Feng, J., Graf, M., Liu, K., Ovchinnikov, D., Dumcenco, D., Heiranian, M., Nandigana, V., Aluru, N.R., Kis, A., and Radenovic, A. (2016). Single-layer MoS2 nanopores as nanopower generators. Nature *536*, 197–200. https://doi.org/10.1038/nature18593.

54. Chen, C., Liu, D., He, L., Razal, J.M., Nicholas, A., Chen, C., Liu, D., He, L., Qin, S., Wang, J., et al. (2019). Bio-inspired Nanocomposite Membranes for Osmotic Energy Harvesting Bio-Inspired Nanocomposite Membranes for Osmotic Energy Harvesting, pp. 247–261. https://doi.org/10.1016/j.joule.2019.11.010.

55. Graf, M., Lihter, M., Unuchek, D., Sarathy, A., Leburton, J.P., Kis, A., and Radenovic, A. (2019). Light-Enhanced Blue Energy Generation Using MoS2 Nanopores. Joule *3*, 1549–1564. https://doi.org/10.1016/j.joule.2019.04.011.

56. Chen, Y.T., Tsou, T.Y., and Hsu, J.P. (2022). Improving the performance of salinity gradient power generation by a negative pressure difference. J. Taiwan Inst. Chem. Eng. *134*, 104351. https://doi.org/10.1016/j.jtice.2022.104351.

57. Vermaas, D.A., Veerman, J., Saakes, M., and Nijmeijer, K. (2014). Influence of multivalent ions on renewable energy generation in reverse electrodialysis. Energy Environ. Sci. *7*, 1434–1445. https://doi.org/10.1039/c3ee43501f.

58. Qiu, Y., Ma, L., Zhuang, J., and Song, F. (2022). Influences of Divalent Ions in Natural Seawater/River Water on Nanofluidic Osmotic Energy Generation. SSRN Journal. https://doi.org/10.2139/ssrn.4064467.

59. Yang, J., Tu, B., Zhang, G., Liu, P., Hu, K., Wang, J., Yan, Z., Huang, Z., Fang, M., Hou, J., et al. (2022). Advancing osmotic power generation by covalent organic framework monolayer. Nat. Nanotechnol. *17*, 622–628. https://doi.org/10.1038/s41565-022-01110-7.

60. Haynes, W.M., Lide, D.R., and Bruno, T.J. (2016). CRC Hand Book of Chemistry and Physics (CRC press).

61. Besha, A.T., Tsehaye, M.T., Aili, D., Zhang, W., and Tufa, R.A. (2019). Design of monovalent ion selective membranes for reducing the impacts of multivalent ions in reverse electrodialysis. Membranes *10*, 7. https://doi.org/10.3390/membranes10010007.

STAR★METHODS

KEY RESOURCES TABLE

REAGENT or RESOURCE	SOURCE	IDENTIFIER
Software and algorithms		
COMSOL Multiphysics 5.6		https://cn.comsol.com/; RRID: SCR_014767
Origin 2021	Northampton, Massachusetts, USA.	https://www.originlab.com/; RRID: SCR_014212

RESOURCE AVAILABILITY

Lead contact

Further information and requests for resources and reagents should be directed to and will be fulfilled by the lead contact, Minyi Xu (xuminyi@dlmu.edu.cn).

Data and code availability

- All data reported in this paper will be shared by the lead contact upon request.
- This paper does not report original code.
- Any additional information required to reanalyze the data reported in this paper is available from the lead contact upon request.

METHOD DETAILS

We use COMSOL Multiphysics 5.6 to study steady-state RED process, using finite element analysis (FEA) method, to understand the superiority of bipolar ionic diode in salinity gradient energy harvesting. For the selection of model parameters, we confirm the main three types of parameters as the key research objects of this simulation by finding out the basic characteristics of nanochannels and the main influencing parameters of RED system.

Physical modeling

According to the characteristics of the RED system, we first construct a geometric model, as shown in Figure 1A. Secondly, by coupling the electric field, ion converse and flow field, the physical field construction of the model is realized. Finally, we completed the construction of all models by drawing the grid. More details about model building can be seen in the section of methods and numerical setup and SI-1. Meanwhile, in order to verify the reliability of the model data, we conducted a grid independence verification, more details can be seen in the SI-3.

Data processing

By drawing the equivalent circuit diagram of the RED system, it is clear that the current and voltage of the system have a linear relationship when different V_C are input. Therefore, by fitting the obtained different V_C and I, the V_0 and R_C of the RED system can generate can be obtained, and the power output of the RED system can also be generated. More details about data processing can be seen SI-2.